Annals of the Academy of Romanian Scientists
Series on Physics and Chemistry
ISSN 2559-1061 Volume **3**, Number **1**/**2018**

HETEROSTRUCTURES BASED ON ORGANIC SEMICONDUCTORS FOR PHOTOVOLTAIC CELLS: STRUCTURAL, OPTICAL AND ELECTRICAL PROPERTIES

Carmen BREAZU[1]
Scientific coordinator: Prof. Univ. Dr. Daniela DRAGOMAN[2]
September 2017

1. Introduction

Reducing primary non-renewable energy source and long-term adverse effects on the environment due to their exploitation determines the need to develop new strategies to efficiently use other primary energy sources, namely renewable ones. Among the natural renewable energies, the sun is a viable alternative, generating 3.8×10^{26} Watts of brightness, which would meet the demand for energy for world consumption per year (1.5×10^{27} Wh in 2015) [1].

The discovery of electrical conduction in organic materials, initially assumed to be insulating, has opened up a very interesting field. This category of materials is characterized by properties that radically differentiate them from inorganic materials and justify their study for photovoltaic and optoelectronic applications.

Photovoltaic cells based on organic thin films offer an attractive direction of research due to photoexcitation and transfer charges phenomena that are hosted by organic molecules. The main challenges are related to optimizing the properties of organic materials (oligomers, polymers, low molecular weight materials) in order to ensure the absorption of a wide spectrum of solar radiation and to control the factors affecting the processes taking place at the interfaces, including the interfaces between the components of the active medium and external contacts [2].

The main objectives of this thesis are the investigation of structural, optical and electrical properties of some thin films based on different organic materials (small molecules, oligomers, polimers) in various configurations in order to improve the performances of devices based on these structures, in particular photovoltaic cells. The efficiency of solar energy conversion can be improved by using an active layer with a morphology characterized by the increase of the contact surface between donors and acceptors, which provides an improved collection of photogenereated charges.

[1]National Institute of Materials Physics, 405 Bis Atomistilor Street, Magurele, Romania.
[2]University of Bucharest, Faculty of Physics, 405 Atomistilor Street, Magurele, Romania, and Academy of Romanian Scientists, 54 Splaiul Independentei, Bucharest, Romania.

2. Bulk heterojunctions based on arylene compounds

The current organic solar cells that present the best conversion efficiency are those with bulk heterojunctions between two semiconductor materials, an electron donor, such as a polymer, oligomer or small molecular material, and an electron acceptor such as fullerene or its derivatives, in a sandwich configuration between two electrodes, one transparent conductive and one metallic, as in Fig. 2.1.

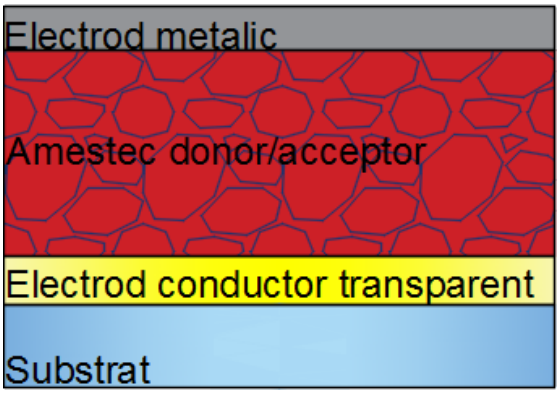

Fig. 2.1. Bulk heterojuction organic solar cell configuration.

The synthesis of new donor materials with optimized absorption spectra, transport properties and energetic levels is a way to improve the performance of photovoltaic cells [3,4].

2.1. Heterostructures based on star-shaped arylenevinylene compounds

One set of heterostructures were made from a mixed layer of 4, 4', 4''-tris [(4'-diphenylamino)-styryl] triphenylamine/IT77 and a fullerene derivative, [6]-phenyl C61 butyric acid butyl ester/PCBB, obtained by MAPLE method. Mixed layers were prepared on glass, glass coated with ITO or silicon substrates, as shown in Table 1.

A buffer film placed between the ITO electrode and the active layer can improve the parameters of organic solar cells with bulk heterojunctions.

A new poly (aniline-co-aniline propane sulfonic acid/copolymer An-AnPs) buffer layer has been proposed, being characterized by an adequate position of energetic levels to favor charge injection/collection from the ITO electrode.

The AFM images of An-AnPs copolymer film deposited on glass/ITO substrate have revealed a large hill-like typical morphology, as can be seen in Fig. 2.1.1a.

The lowest roughness is observed in the mixed layers deposited on glass/ITO substrate, and the highest roughness is shown by the sample prepared on An-AnPS copolymer film [5].

Table 1. Organic layers preparation conditions

Sample	Structure	Fluence (mJ/cm^2)	No. of pulses
O1	Glass/IT77	300	5000
M1	Glass/IT77:PCBB	250	8000
M2	Si/IT77:PCBB	250	8000
P2	Glass/ITO/film2/IT77:PCBB	250	8000
P6	Glass/ITO/film6/IT77:PCBB	250	8000
P8	Glass/ITO/film8/IT77:PCBB	250	8000
P11	Glass/ITO/ IT77:PCBB	250	10000
P13	Glass/ITO/PEDOT:PSS/IT77:PCBB	250	10000
P15	Glass/ITO/PEDOT:PSS/IT77:PCBB	250	12000
P16	Glass/ITO/ IT77:PCBB	250	12000
S2	Glass/ITO/An-AnPS	Electrochemical polymerization	
S6	Glass/ITO/An-AnPS	Electrochemical polymerization	
S8	Glass/ITO/An-AnPS	Electrochemical polymerization	
DC	Si/IT77:PCBB	Dropcast	

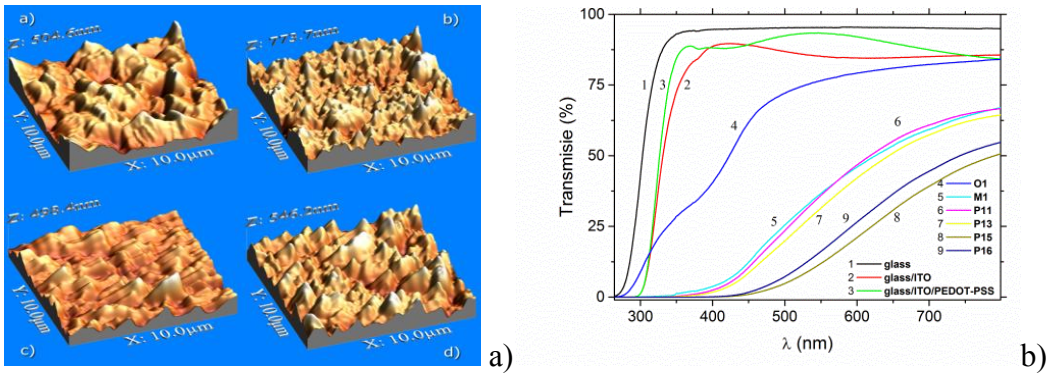

a) b)

Fig.2.1.1. a) AFM Images: a) An-AnPS deposited on glass/ITO substrate, b) IT77:PCBB deposited on glass/ITO/An-AnPS substrat, c) IT77:PCBB deposited on glass/ITO substrate, d) IT77:PCBB deposited on glass/ITO/PEDOT:PSS substrate; b) UV-Vis spectra of thin films prepared with IT77 and IT77 with fullerene [5]

The UV-Vis spectra (Fig. 2.1.1b) revealed the effect of the fullerene on the optical properties of thin films based on the star-shaped compound.

The spectrum of the reference sample (O1) prepared on a glass substrate of IT77 compound revealed a good transmission at wavelengths greater than 500 nm.

The addition of PCBB to the IT77 compound (M1 sample) was observed to shift the fundamental absorption edge from ~270 nm to above 370 nm, as illustrated in Fig. 2.1.2 [5].

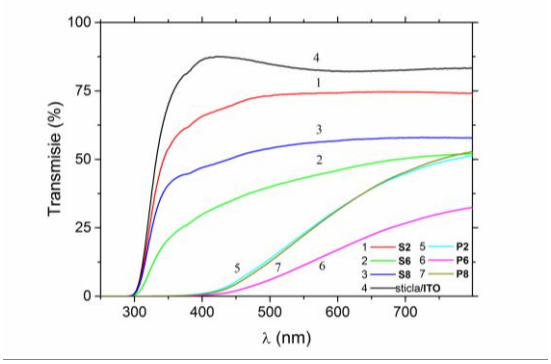

Fig.2.1.2. UV-Vis spectra of thin films prepared with IT77 and IT77:PCBB: S2, S6, S8, P2, P6, P8.

We have investigated the I-V characteristics of the organic heterostructures with mixed layers realized with An-AnPs copolymer or PEDOT:PSS buffer layer in comparison with I-V characteristics of the organic heterostructures realized without buffer layer.

Samples P2 and P16 (Fig. 2.1.3b) have shown an injection contact behavior and a small asymmetry. The best injection of charge carriers is evidenced in sample P16, ~70 μA at 1 V.

Solar cell behavior has observed in the sample P13 (Fig. 2.1.3a) characterized by the following parameters: V_{OC} = 0.34 V, I_{SC} = 1.98 nA and FF = 0.29.

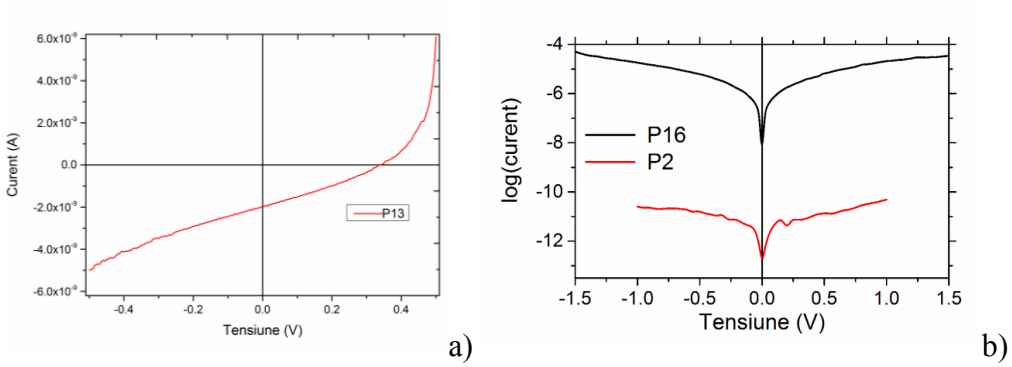

Fig.2.1.3. I-V characteristics for: a) P13-glass/ITO/PEDOT:PSS/IT77:PCBB/Al; b) P2- glass/ITO/An-AnPS/IT77:PCBB/Cu, P16-glass/ITO/IT77:PCBB/Cu [5]

2.2. Heterostructures with polymers based on arylene

Other materials investigated were polymers based on arylene, poly[N-(2-ethylhexyl)2.7-carbazolylvinyl]/AMC16 and poly[N-(2-ethylhexyl) 2.7 carbazolyl 1.4 pheylene ethynylene]/AMC22. The studied heterostructures were made of a simple polymer layer, or a mixed layer of polymer and C60-fullerene. The active layers were deposited on the substrate by MAPLE technique using chloroform as solvent.

AFM images (Figs. 2.2.1 and 2.2.2) of the realized films with AMC 16 and AMC 22 polymers show a globular morphology of both single and mixed polymers films made with fullerene [6]. We assumed that these granulations contain both polymer and fullerene. It has been observed that the addition of fullerene to the polymer does not affect the morphology of the films.

The UV-VIS spectra have revealed the effect of fullerene C60 on the optical properties of AMC 16 and AMC 22 films deposited on different substrates. The spectra of the mixed polymer:C60 layers are not the superposition of the spectra of individual components, meaning that some changes occurred during deposition of films containing fullerene, which affected the electronic properties [7].

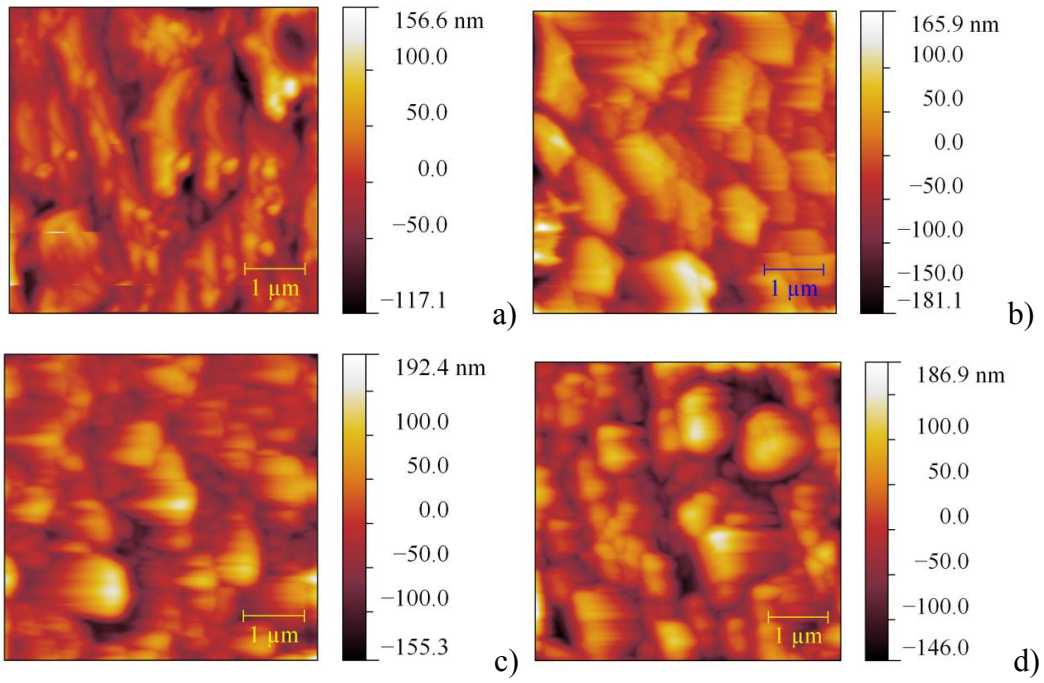

Fig.2.2.1. AFM images: a) polymer AMC16 film deposited on glass/ITO substrate; b) polymer AMC16:C60 film deposited on glass/ITO substrate; c) polymer AMC22 film deposited on glass/ITO substrate; d) polymer AMC22:C60 film deposited on glass/ITO substrate [6].

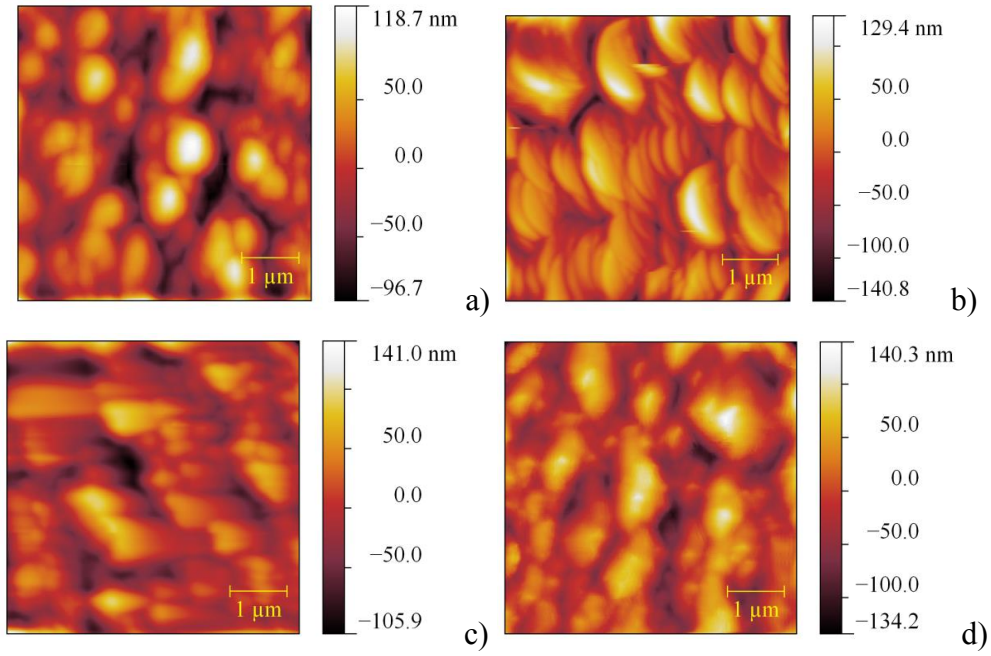

Fig.2.2.2. AFM Images: a) polymer AMC16 film deposited on glass/ITO/PEDOT:PSS substrate; b) polymer AMC16:C60 film deposited on glass/ITO/PEDOT:PSS substrate; c) polymer AMC22 film deposited on glass/ITO/PEDOT:PSS substrate; d) polymer AMC22:C60 film deposited on glass/ITO/ PEDOT:PSS substrate [6].

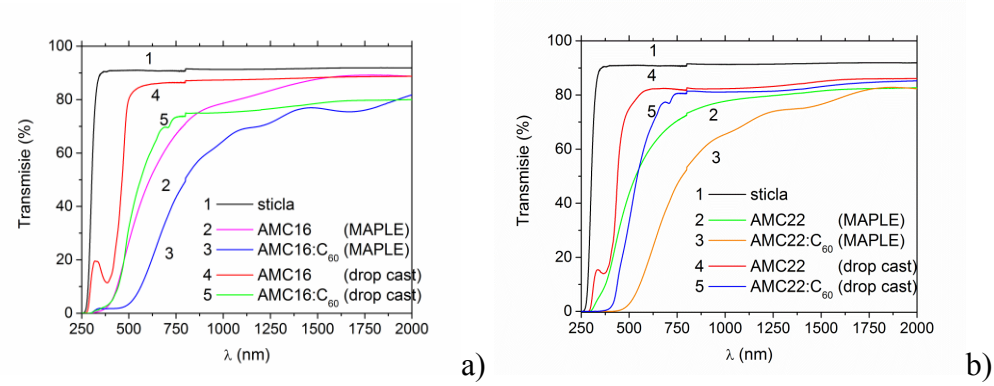

Fig.2.2.3. UV-Vis spectra of polymeric films: a) AMC16 and b) AMC22 and a mixed layers polymer:fulerene realized by MAPLE and dropcast [6]

The reference samples prepared on glass substrate by dropcast show good transmission, over 80% at wavelengths higher than 550 nm (see Fig. 2.2.3). By adding fullerene, the fundamental absorption edge is slightly shifted to red, both in samples prepared on glass/ITO and glass/ITO/PEDOT:PSS substrates (Fig. 2.2.4) [6].

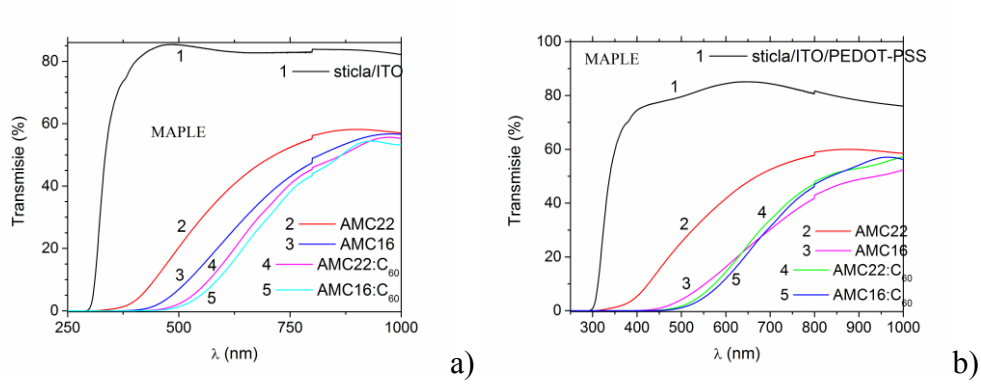

Fig.2.2.4. UV-Vis spectra of polymeric films and mixed layers: a) AMC16 and AMC22 deposited by MAPLE on glass/ITO substrate; b) AMC16 and AMC22 deposited by MAPLE on glass/ITO/PEDOT:PSS substrate [6].

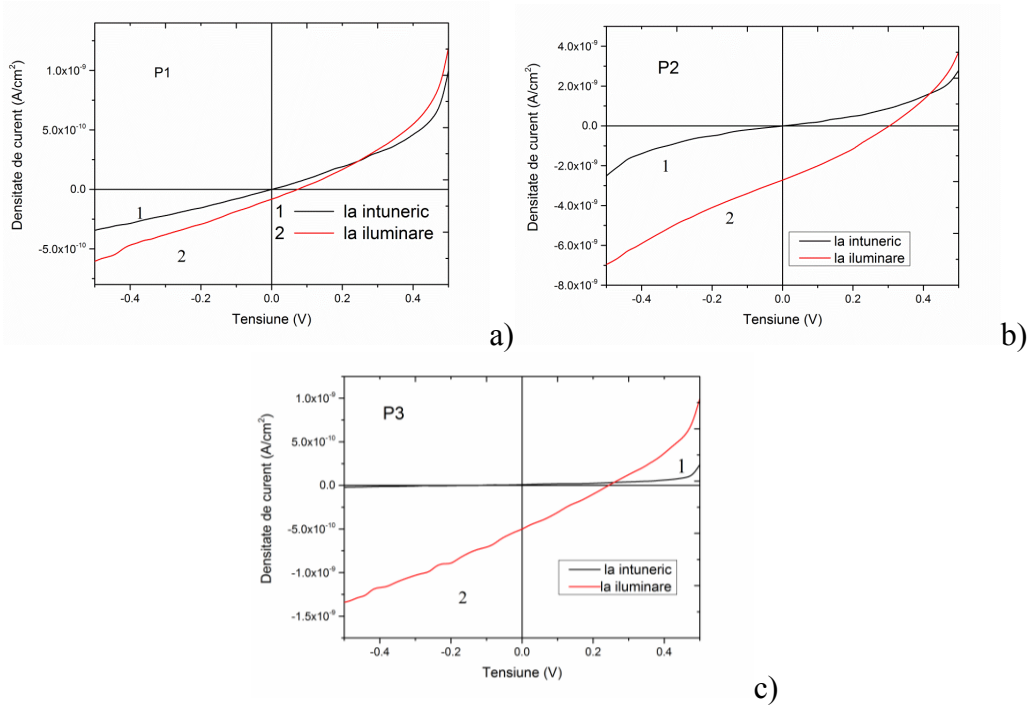

Fig.2.2.5. I-V characteristics for structures: a) P1: glass/ITO/PEDOT:PSS/AMC22/Al, b) P2:glass/ITO/PEDOT:PSS/AMC16/Al, c) P3: glass/ITO/PEDOT:PSS/AMC22:C60/Al [6].

Photovoltaic effect has shown the sample with polymer AMC16, AMC22 and AMC22:C60 (Fig. 2.2.5) deposited on glass/ITO/PEDOT:PSS. The highest current density at illumination was obtained in the P3 sample, which contains the mixed active layer with polymer AMC 22 and fullerene and buffer layer PEDOT:PSS.

3. Photonic crystals

The advances in ceramic, plastics and metallurgy have allowed the control of mechanical properties of materials, the advances in semiconductor physics have allowed the control of electrical conduction properties, and in recent decades the advances in the field of photonic crystals have allowed the control of optical properties of materials [8]. The opportunity to control the emission and light extraction using photonic crystals offers a vast potential to improve existing light sources. Of interest are photonic crystals possessing a completely forbidden band (for both polarizations TE, TM), similar to the forbidden band formed between the valence and conduction bands in a semiconductor [9].

3.1 The bandstructure for TM polarization of different 2D photonic crystals

We applied the PWE method to calculate the eigenfrequencies of a 2D photonic crystals composed of cylindrical, square, triangular, hexagonal or octagonal cross-section dielectric rod shapes arranged in a periodic square structure.

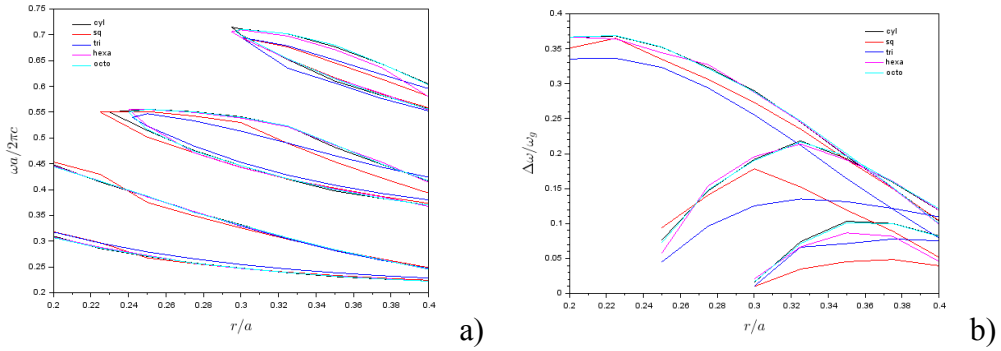

Fig.3.1.1. a) The first three TM bandgaps as a function of r/a for PBGs consisting of rods with ε = 11 in air with cylindrical, square, triangular, hexagonal and octagonal cross-sections; b) The coresponding dependences of the ratio between the width and the central bandgap position [10].

The difference in the position and width of bandgaps increases with the number of the bands. For all three bands in Fig. 3.1.1 the position and width of the forbidden band for hexagonal and cylindrical rods are impossible to distinguish due to the similarity in shape of the rods [10]. Otherwise, photonic crystals with square and triangular rods, in which field distributions are different from that in cylindrical rods, show high difference in the position and width of the bands. This behavior can be understood from the distribution of the magnetic field in photonic crystals of different rod shapes. The magnetic field of the photonic crystal with square and triangular rods has different shapes compared to that in periodic structures with cylindrical rods, while the field distribution in the crystals with hexagonal and octagonal rods is very similar to the cylindrical rod structure [10]. This is the reason why the position and width of the bandgaps in photonic crystals with triangular and square rods differ most from the cylindrical rods (Fig. 3.1.2) [10].

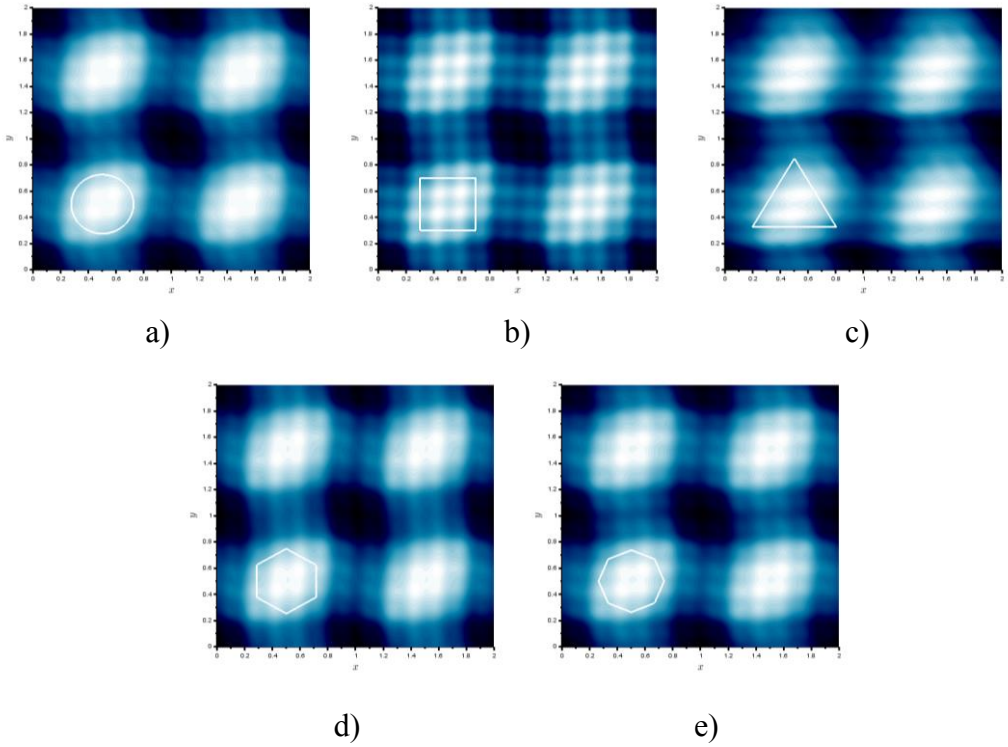

Fig. 3.1.2. Magnetic field distribution for the first TM mode in the M point of the first Brillouin zone of the square lattice with r/a = 0.225 and ε = 11, for:
a) cylindrical, b) square, c) triangular, d) hexagonal, e) octagonal [10].

3.2 Organic heterostructures prepared on nanostructured metallic electrod

Such two-dimensional periodic structures have been obtained using the nanoimprint technique.

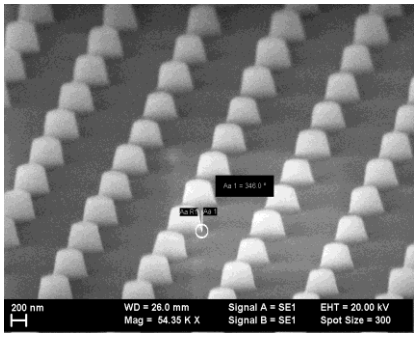

Fig. 3.2.1. SEM image of patterned photoresist on Si substrate [11]

In the addition to the synthesis of new organic materials, the development of different configurations is an alternative for making devices with improved performances. A solution for improving the mobility of charge carriers consists in nanostructuring the metallic electrodes, which leads to the creation of an intense electric field in the regions with a smaller curvature and in the change of the contact area between the active layer and the metal electrode, which favors the injection/collection of carriers [12-15].

Organic heterostructures were made from small molecule organic semiconductors. The active layer consisted of a p-type semiconductor, ZnPc, and a n-type semiconductor, C60. A buffer layer of NTCDA, which does not absorb in the visible spectrum, has been used as hole blocking layer [16]. The metallic electrode, Al (planar or nanostructured) was deposited on a Si substrate, and the transparent electrode was positioned at the top of the structures.

The heterostructures as a whole were fabricated with masks. Therefore, the form of the reflection spectra (Fig. 3.2.2) is the result of overlapping reflections of the ZnO film deposited in the top of structures with the ZnPc and C60 film reflection and that of the planar or nanostructured Al electrode. In the heterostructures with triple organic layers of NTCDA/C60/ZnPc, the patterned memory is not preserved and a slightly increased and fluctuating reflectance is observed [17].

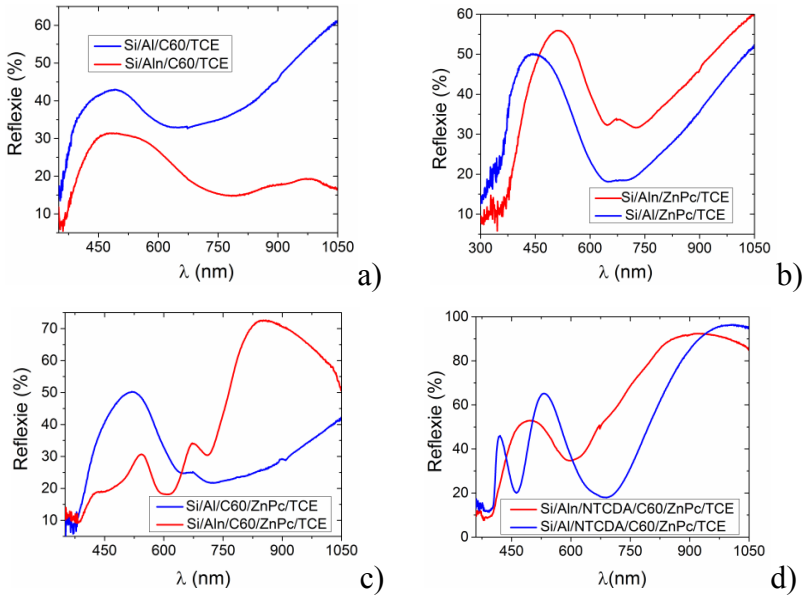

Fig.3.2.2. Reflectance spectra of single/multi-layer organic heterostructures [18]

The photoluminescence spectra of single/multi-layer organic heterostructures (Fig. 3.2.3) with nanostructured metallic electrodes are dominated by the nanostructured Al [11]. At excitation with λ = 335 nm, most of heterostructures

realized on planar metallic electrodes show a weak peak situated at about 500 nm, which can be correlated with resonance phenomena between the incident radiation and surface plasmons generated in the Al layer. By nanostructuring the Al film, this phenomenon became intense and the shape of the emission spectra is affected, highlighting an integer peak at about 510 nm and a weaker one at 595 nm. At excitation with λ = 435 nm, the shape of the emission spectra is preserved for the heterostructures obtained on both planar and nanostructured Al, showing a maximum emission at about 595 nm [18].

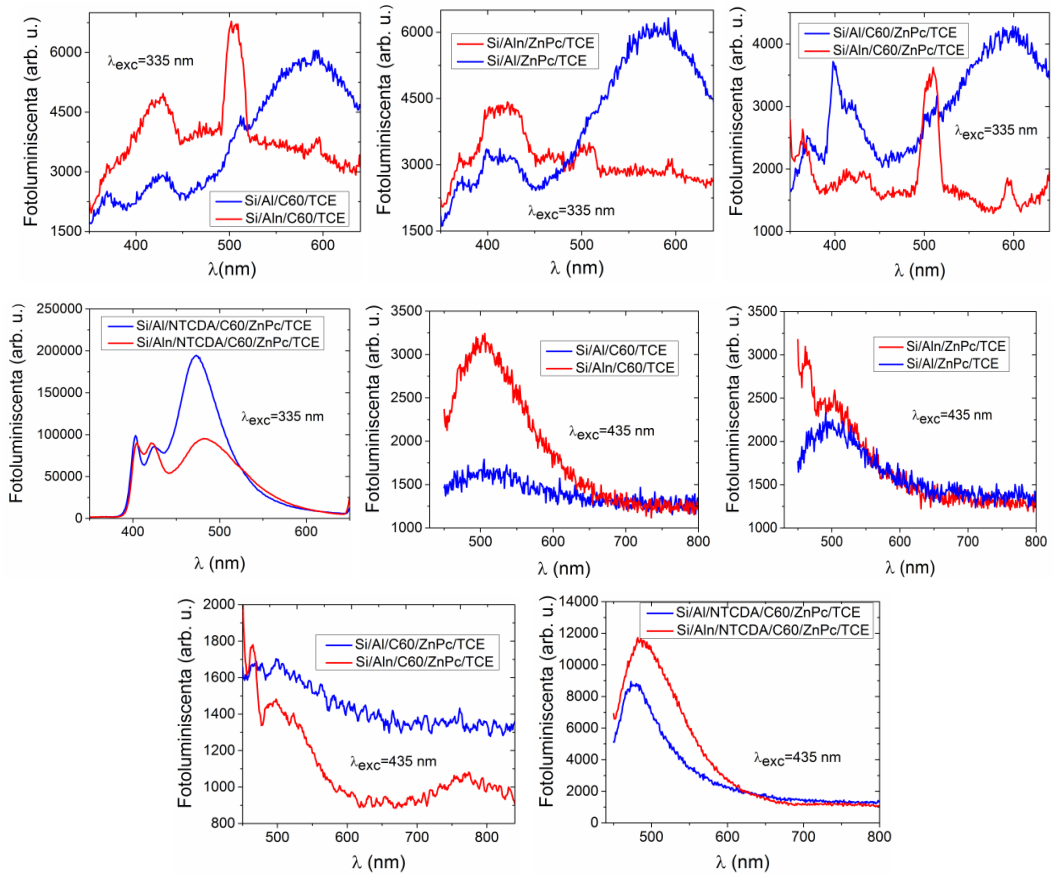

Fig.3.2.3. The emission spectra of single/multi-layer organic heterostructures [18].

An injection contact behavior was evidence for most heterostructures built on flat and patterned Al (Fig. 3.2.4) [18]. At a voltage of 0.6 V the current is significant, about 10^{-5} A in the Si/Al/ ZnPc/ZnO/Au/ZnO structure. The increase in current is determinated by changes in the electronic properties of ZnPc molecules due to strong ZnPc/ZnO coupling [19]. Nanostructuring of the Al electrode leads to an increase in current (~$4x10^{-5}$ A) for a voltage of 0.6 V. The heterostructure with C60 shows a current of $6x10^{-7}$ A at 0.25 V, its behavior remaining unaffected by nanostructuring of the Al electrode [18].

The sample Si/Al/C60/ZnPc/ ZnO/Au/ZnO shows an asymmetric non-linear injector contact behavior with a current of ~5×10^{-6} A at 1 V. The heterostructure with triple organic layer is characterized by a current of $4x10^{-4}$ A at 0.7 V. A change in shape of the I-V characteristics was highlighted in the same structure with nanostructured metallic electrode.

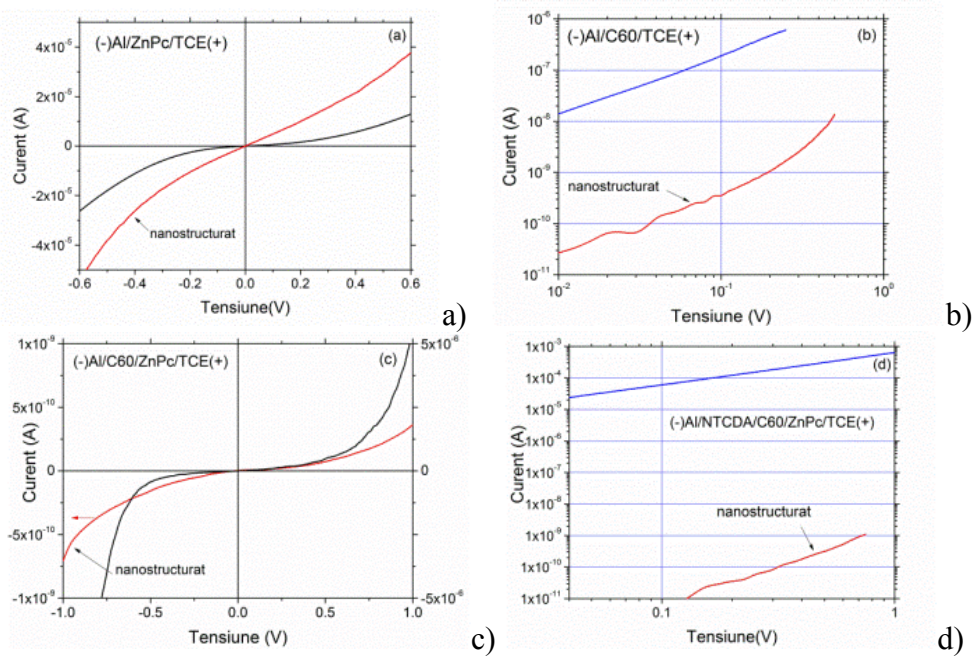

Fig.3.2.4. I-V characteristics of the organic heterostructures prepared on planar and nanostructured metallic electrodes [18].

6. Conclusions

To improve the performance of organic solar cells, in this thesis, we have investigated several organic thin films (based on polymers and oligomers) in various configurations, the molecular packaging being an important factor that affects the properties of organic heterostructures. Thus, active layers were prepared by the MAPLE technique on different substrates, such as flexible ones, glass, glass/ITO, Si, resulting in different thicknesess and morphologies depending on experimental conditions. The physical properties of organic heterostructures have been evidenced by structural, morphological, optical and electrical measurements. All the sample show good transmission, 70-80%. Using PWE method we calculated the eigenfrequencies of 2D photonic crystals composed of cylindrical, square, triangular, hexagonal and octagonal cross-section dielectric rods arranged in a periodic square structure. Such periodic nanostructures could have been obtained experimentally by nanoimprint lithography. As a result of I-V measurements, several heterostructures showed photovoltaic effect, which confirms that these organic materials based on arylene compounds can be used as active layers in the production of photovoltaic cells.

R E F E R E N C E S

[1] http://energyinformative.org/nrel-efficiency-record-two-junction-solar-cell

[2] A. E. Becquerel, (1839) Mémoire sur les effets électriques produits sous l'influence des rayon solaires, Compt. Rend. Acad. Sci. 9, 561.

[3] A. Stanculescu, O. Raşoga, M. Socol, L. Vacareanu, M. Grigoras, G. Socol, F. Stanculescu, E. Matei, N. Preda, M. Girtan (2017) MAPLE prepared heterostructures with oligoazomethine: Fullerene derivative mixed layer for photovoltaic applications, Appl. Surf. Sci. 417, 183-195.

[4] A. Stanculescu, G. Socol, L. Vacareanu, M. Socol, O. Rasoga, C. Breazu, M. Girtan, F. Stanculescu (2016) MAPLE preparation and characterization of mixed arylenevinylene based oligomers:C60 layers, Appl. Surf. Sci. 374, 278-289.

[5] A. Stanculescu, G. Socol, G. Grigoras, T. Ivan, L. Vacareanu, M. Socol, O. Rasoga, C. Breazu, I. N. Mihailescu, I. Iordache, N. Preda, F. Stanculescu (2014) Laser prepared organic heterostructures based on star-shaped arylenevynilene compounds 117, Applied Physics A, 261-268.

[6] F. Stanculescu, O. Rasoga, A. M. Catargiu, L. Vacareanu, M. Socol, C. Breazu, N. Preda, G. Socol, A. Stanculescu (2015) MAPLE prepared heterostructures with arylene based polymer active layer for photovoltaic applications, Appl. Surf. Sci. 336, 240-248.

[7] B. M. Omer (2013) Optical properties of Poly(3-hexylthiophene-2, 5-diyl) and Poly (3-hexylthiophene-2, 5-diyl)/[6,6]-Phenyl C61-butyric acid 3-ethylthiophene ester thin films, J. Nano. Electron. Phys. 5, 03011-03014.

[8] G. R. Bhimanapati, Z. Lin, V. Meunier, Y. Jung, J. Cha, S. Das, Di. Xiao, Y. Son, M. M. Strano, V. R. Cooper, L. Liang, S. G. Louie, E. Ringe, W. Zhou, S. S. Kim, R. R. Naik, B. G. Sumter, H. Terrones, F. Xia, Y. Wang, J. Zhu, D. Akinwande, N. Alem, J. A. Schuller, R. E. Schaak, M. Terrones, J. A. Robinson (2015) Recent advances in two-dimensional materials beyond graphene, ACS Nano. 9, 11509-11539.

[9] R. Antos, M. Veis (2012) Photonic Crystals-Introduction, Applications and Theory, INTECH.

[10] D. Dragoman, C. Breazu (2017) Fault-tolerant bandstructure of two-dimensional square photonic crystals with different dielectric rod shapes, Photonic. Nanostruct. 24, 12-17.

[11] C. Breazu, N. Preda, M. Socol, F. Stanculescu, E. Matei, I. Stavarache, G. Iordache, M. Girtan, O.Rasoga, A. Stanculescu (2016), Investigations of the properties of a two- dimensional nanopatterned metallic film, Dig. J. Nanomater. Bios. 11, 1213-1229.

[12] M. Fina, S. S. Mao (2012) Approximating the electrical enhancement effects in a nano-patterned, injection-limited, single-layer organic light-emitting diode, Appl. Phys. Lett. 112, 024512/1-12.

[13] L.-J. Pegg, R. A. Hatton (2012) Nanoscale geometric electric field enhancement in organic photovoltaics, ACS Nano, 6, 4722–4730.

[14] M.-H. Hsu, P. Yu, J.-H. Huang, C.-H. Chang, C.-W. Wu, Y.-C. Cheng, C.-W. Chu (2011) Balanced carrier transport in organic solar cells employing embedded indium-tin oxide nanoelectrodes, Appl. Phys. Lett. 98, 073308/1-3.

[15] R. B. Dunbar, T. Pdflaer, L. Schmidt-Mende (2012) Highly absorbing solar cells of survey of plasmonic nanostructures, Opt. Express 20, A117-A189.

[16] C. Falkenberg, C. Uhrich, S. Olthof, B. Maennig, M. K. Riede, K. Leo (2008) Efficient *p-i-n* type organic solar cells incorporating 1,4,5,8-naphthalene- tetracarboxylic dianhydride as transparent electron transport material, J. Appl. Phys. 104, 034506/1-6.

[17] J. M. Ha, S. H. Yoo, J. H. Cho, Y. H. Cho, S. H. Cho (2014) Enhancement of antireflection property or silicon using nanostructured surface combined with a polymer deposition, Nanoscale Res. Lett. 9, 9/1-5.

[18] C. Breazu, M. Socol, N. Preda, E. Matei, O. Rasoga, M. Girtan, R. Mallet, F. Stanculescu, A. Stanculescu (2018) On the properties of organic heterostructures prepared with nanopatterned metallic electrode, Appl. Surf. Sci., in press, https://doi.org/10.1016/j.apsusc.2018.02.103.

[19] G. Mattioli, S. B. Dkhil, M. I. Saba, G. MAlloci, C. Melis, P. Alippi, F. Filippone, P. Giannozzi, A. K. Thakur, M. Gaucer, O. Margeat, A. K. Diallo, C. Videlot-Ackmann, J. Ackemann, A. A. Bonapasta, A. Mattoni (2014) Interfacial engineering of P3HT/ZnO hybrid solar cells using phtalocyanines: A joint theoretical and experimental investigation, Adv. Energy Mater. 4, 1301694/1-11.